www.sciencemag.org/cgi/content/full/328/5974/67/DC1

Supporting Online Material for

A Gating Charge Transfer Center in Voltage Sensors

Xiao Tao, Alice Lee, Walrati Limapichat, Dennis A. Dougherty, Roderick MacKinnon*

*To whom correspondence should be addressed. E-mail: mackinn@rockefeller.edu

Published 2 April 2010, *Science* **328**, 67 (2010)
DOI: 10.1126/science.1185954

This PDF file includes

Supporting Online Materials

Materials and Methods

Mutagenesis

All the mutants were generated using the QuikChange site-directed mutagenesis kit (Stratagene) and incorporation of the mutation(s) was verified by sequencing (GeneWiz).

Expression, purification, and crystallization of the F233W mutant of Kv2.1 paddle-Kv1.2 chimera channel

The F233W mutant of Kv2.1 paddle-Kv1.2 chimera channel was expressed and purified the same way as described for the wild-type chimera channel (*1*). In brief, the channel was co-expressed with the rat β2-core gene in *Pichia pastoris*, extracted with DDM (n-dodecyl-β-D-maltopyranoside, Anatrace), and purified on a cobalt affinity column followed by gel filtration on a Superdex-200 column. Protein was concentrated to 10 mg/ml (Centricon-50, Millipore), mixed (0.4 µl + 0.4 µl) with crystallization solution and crystallized using the hanging drop vapor diffusion method over reservoirs containing 0.1 ml crystallization solution at 20°C. The crystallization solution contained 25-28% PEG400 and 50 mM TRIS-HCl pH 8.3-8.9. Crystals appeared within 1-3 days and were approximately 100*100*50 µm in size.

Structure determination

Crystals were directly frozen in liquid nitrogen after overnight equilibration against a reservoir solution containing 33% PEG400 and 50 mM TRIS-HCl pH 8.5. Diffraction data were collected to 2.9 Å at beamline X29 (Brookhaven NSLS), images processed with DENZO and intensities merged with SCALEPACK (*2*). Data were further processed using the CCP4 suite (*3*). The crystals are isomorphous to the wild-type paddle chimera channel, belonging to the P4212 space group. The wild type structural model (PDB ID 2R9R) with Phe233 replaced by alanine was used as a starting model. Iterative refinement with CNS (keeping the same test set as wild type) (*4*) and manual rebuilding using O (*5*) generated a final model with residual R-free of 24.7%. The final model contains: β2.1 residues 36-361, paddle chimera channel residues 29-417. All side chains are included in the model with the exception of channel residues 133-144 (the link between T1 and the transmembrane region) which was modeled as poly-glycine. Crystallographic data and refinement statistics are shown in supplementary information (Table S1). Figures were made using PYMOL (www.pymol.org) (*6*).

Shaker K+ channel expression

The Shaker H4 (inactivation removed) construct in a BlueScript vector was used for Shaker K+ channel expression in *Xenopus* oocytes (*7*). The N-type inactivation gate (corresponding to amino acids 6-46) was not included in the construct (*8*). cRNA was prepared from HindIII linearized plasmid using T7 RNA polymerase (Promega).

Xenopus oocytes were harvested from mature female *Xenopus laevis* and defolliculated by collagenase treatment for 1-2 hours. Oocytes were then rinsed thoroughly and stored in ND96 solution (96 mM NaCl, 2 mM KCl, 1.8 mM CaCl2, 1.0 mM MgCl2, 5 mM HEPES, 50 µg/ml gentamycin, pH 7.6 with NaOH). Defolliculated oocytes were selected 2-4 hours after collagenase treatment and injected with cRNA the next day. The injected oocytes were incubated in ND96 solution before recording. Recordings were usually done 1-2 days post-injection for ionic current measurements and 3-6 days post-injection for gating current measurements. All oocytes were stored in an incubator at 18 °C.

Unnatural amino acid incorporation

Unnatural amino acids were incorporated into the Shaker K+ channel using the nonsense codon

suppression method (*9*). THG73 was used as the amber suppressor tRNA (*10*). The preparations of amino acids coupled to the dinucleotide (dCA) and the ligation of the conjugated dCA-amino acid have been described previously (*9*). Crude tRNA-amino acid product was used without desalting, and the product was confirmed by MALDI-TOF MS on 3-hydroxypicolinic acid (3-HPA) matrix. Deprotection of the NVOC group on tRNA-amino acid was carried out by 10-minute photolysis immediately prior to injection. Equal volumes of the Shaker cRNA (in which the codon for Phe was replaced by the amber stop codon) and unprotected tRNA-amino acid were mixed prior to injection. Approximately 15 ng of tRNA was used per oocyte. As a negative control, 76-nucleotide tRNA (dCA ligated to 74-nucleotide tRNA) was co-injected with cRNA in the same manner as fully charged tRNA.

Electrophysiological recordings

All recordings were performed at room temperature in two-electrode voltage-clamp configuration with an oocyte clamp amplifier (OC-725C, Warner Instrument Corp.), Digidata 1440A analogue-to-digital converter interfaced with a computer, and pClamp10.1 software (Axon Instruments, Inc) for controlling membrane voltage and data acquisition. The recorded signal was filtered at 1kHz and sampled at 10kHz.

To investigate voltage-dependent channel activation, oocytes were held at -80 mV (Shaker wt and most of the mutants) or -110 mV [F→W i.e. R1K5(W) mutant] with pulse potential starting from holding potential ending between +30 mV and +180 mV in 10 mV, 5 mV or 2.5 mV increments. The repolarization potentials were either more negative to the voltage at which channel starts to open (for most mutants) or slightly positive to that voltage (for mutants with very fast closure rate). To investigate voltage-dependent channel closure, oocytes were held at -80 mV (Shaker wt and most other mutants) or -110 mV [R1K5(W) mutant], depolarized to between 0 mV and +80 mV with repolarization potentials starting from the depolarization potential ending between -100 mV and -140 mV in 10mV decrements. Recording solution for the above experiments contained 98 mM KCl, 0.3 mM CaCl2, 1 mM MgCl2, and 5 mM HEPES pH 7.6.

For capacitive current measurement, immediately prior to recording, the oocytes were incubated in ND96 recording solution (96 mM NaCl, 2 mM KCl, 0.3 mM CaCl2, 1 mM MgCl2, and 5 mM HEPES pH 7.6) plus 50 to 100 μM Agitoxin2 for 5-10 minutes with gentle rocking. During recording, holding and repolarization potentials were between -80 mV and -110 mV with pulse potentials starting between -160 mV and -200 mV ending between +60 mV and +120 mV.

Data analysis

No leak or capacitive current was subtracted from the current traces of voltage-dependent channel activation and channel closure shown in Figures 2, 3 and 4. For voltage-dependent channel activation recordings, the amount of current at the repolarization step, typically measured 4-5 ms after the depolarization step when most of the capacitive current has relaxed, was normalized against the maximal current (I/I_{max}) and plotted as a function of the depolarization voltage (*I-V* plot). This voltage-dependent activation plot was fitted with the two-state Boltzmann function:

$$\frac{I}{I_{\max}} = \frac{1}{1+\exp\left(-\frac{\mathrm{ZF}}{\mathrm{RT}}\left(V-V_m\right)\right)}$$

where I/I_{max} is the fraction of the maximal current, V is the depolarization voltage to open the channels, V_m is the voltage at which the channels have reached 50% of their maximal current, F is the Faraday's constant, R is the gas constant, T is the absolute temperature, and Z is the apparent valence

of voltage dependence. Note that I/I_{max} does not represent the true open probability (P_o) of the channel, given that the maxium P_o of Shaker wt channel in whole oocytes is less than 1.0 (*11*).

For the transient (capacitive plus gating) current traces shown in Figure 5A-D, Agitoxin2-insensitive currents were subtracted separately for the three steps of the recording: (i) hyperpolarization, (ii) depolarization, and (iii) repolarization. For each step, the leak current was defined as the current measured near the end of the step. The total gating charges, calculated by integrating the repolarization-induced transient currents over time and subtracting the linear component due to the linear capacitance of the cell and the voltage clamp system, are plotted against the depolarization voltage (*Q-V* plot).

All statistical fits and figure plotting were done using Clampfit 10.1 (Axon Instruments, Inc) or Igor Pro 6.03A2 (WaveMetrics, Inc).

Theoretical analysis of voltage sensor states

The theoretical curves in Figure 6 were produced as solutions to the following expressions describing the model of voltage sensor states (Fig. 6A). Forward and backward voltage-dependent rate constants are given by equations (1) and (2), respectively.

$$k_{ij}(v) = k_{ij}(0)\exp(\frac{0.125zFv}{RT}) \quad (1)$$

$$k_{ji}(v) = k_{ji}(0)\exp(-\frac{0.125zFv}{RT}) \quad (2)$$

These equations partition one quarter of the total gating charge per voltage sensor (z) to each transition with one eighth of the total in the forward and one eighth in the backward reaction. The constants R, T, and F are the gas constant, absolute temperature and Faraday's constant, respectively. At membrane voltage *v* the probability *P*i that a voltage sensor is in state i = 1 to 5 was calculated with equations (3) – (8).

$$P_1(v) = [k_{21}(v)k_{32}(v)k_{43}(v)k_{54}(v)]D^{-1} \quad (3)$$

$$P_2(v) = [k_{12}(v)k_{32}(v)k_{43}(v)k_{54}(v)]D^{-1} \quad (4)$$

$$P_3(v) = [k_{12}(v)k_{23}(v)k_{43}(v)k_{54}(v)]D^{-1} \quad (5)$$

$$P_4(v) = [k_{12}(v)k_{23}(v)k_{34}(v)k_{54}(v)]D^{-1} \quad (6)$$

$$P_5(v) = [k_{12}(v)k_{23}(v)k_{34}(v)k_{45}(v)]D^{-1} \quad (7)$$

$$\sum_{i=1}^{5} P_i(v) = 1 \quad (8)$$

The gating charge curves (*Q-V* curves, Fig. 6, C and D solid curves) were calculated with equation (9)

$$\frac{Q}{Q_{max}} = 0.25P_2(v) + 0.5P_3(v) + 0.75P_4(v) + P_5(v) \quad (9)$$

and the current curves (*I-V* curves, Fig. 6, C and D dashed curves) were calculated with equation (10), which approximates channel opening as a power function of voltage sensor state 5.

$$I(v) = [P_5(v)]^4 \quad (10)$$

The gating current time course curves (Fig. 6B) were calculated by first solving differential equations (11) – (15)

$$\frac{dP_1(t,v)}{dt} = k_{21}(v)P_2(t,v) - k_{12}(v)P_1(t,v) \quad (11)$$

$$\frac{dP_2(t,v)}{dt} = k_{12}(v)P_1(t,v) + k_{32}(v)P_3(t,v) - [k_{21}(v) + k_{23}(v)]P_2(t,v) \quad (12)$$

$$\frac{dP_3(t,v)}{dt} = k_{23}(v)P_2(t,v) + k_{43}(v)P_4(t,v) - [k_{32}(v) + k_{34}(v)]P_3(t,v) \quad (13)$$

$$\frac{dP_4(t,v)}{dt} = k_{34}(v)P_3(t,v) + k_{54}(v)P_5(t,v) - [k_{43}(v) + k_{45}(v)]P_4(t,v) \quad (14)$$

$$P_5(t,v) = 1 - \sum_{i=1}^{4} P_i(t,v) \quad (15)$$

with initial values given by equations (3) – (7) and v = membrane voltage prior to the voltage step. The gating current in units of elementary charge units per second as a function of time was then calculated with equation (16), which describes the time-dependent flux of voltage sensor states in the forward direction.

$$\frac{dQ}{dt} = 0.25z\{[k_{12}(v)P_1(t,v) - k_{21}(v)P_2(t,v)] + [k_{23}(v)P_2(t,v) - k_{32}(v)P_3(t,v)]$$
$$+[k_{34}(v)P_3(t,v) - k_{43}(v)P_4(t,v)] + [k_{45}(v)P_4(t,v) - k_{54}(v)P_5(t,v)]\} \quad (16)$$

The total gating charge per voltage sensor (z) was assigned the value 3.5 elementary charge units (*12*). For the R1K5(W) channel (Fig. 6, B and C) zero-voltage rate constants were $k12(0) = k23(0) = k34(0) = 1500$ sec-1, $k21(0) = k32(0) = k43(0) = 100$ sec-1, $k45(0) = 150$ sec-1, $k54(0) = 10$ sec-1. For the R1R5(W) channel (Fig. 6, B and D) zero-voltage rate constants were the same except $k54(0) = 1000$ sec-1. All equations were solved using Maple 12.0 (Maplesoft). The differential equations were solved numerically using the Runge-Kutta Fehlberg method to fifth order accuracy.

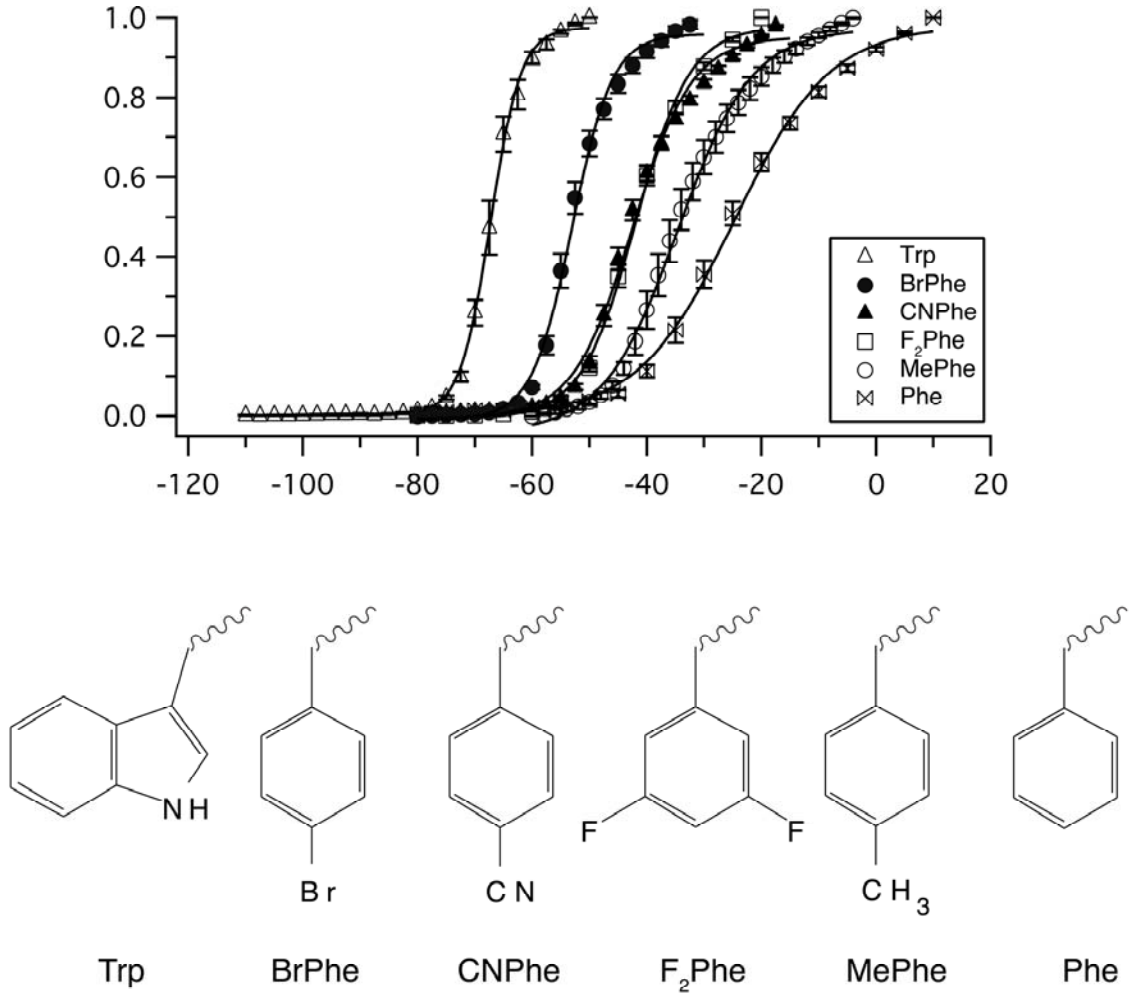

Fig. S1. The voltage-dependent channel activation curves are shown for Phe (Shaker wt) and Phe to 3,5-F-Phe (F_2Phe), 4-bromo-Phe (BrPhe), 4-cyano-Phe (CNPhe), 4-methyl-Phe (MePhe), Trp mutants. Fraction of the maximal current (I/I_{max}, mean ± s.e.m.) is plotted as a function of the depolarization voltage and fitted with the two-state Boltzmann function (see methods, Phe, n = 11; F_2Phe, n = 14; BrPhe, n= 10; CNPhe, n = 5; MePhe, n= 6 and Trp, n =9). The cation-π binding energy in kcal/mol: Trp -32.6, MePhe -28.5, BrPhe -27.6, Phe -27.1, F_2Phe -17.1 and CNPhe -15.7 (*13*). More negative binding energy means stronger cation-π interaction. Chemical structures of the side chains are shown below the I-V plot.

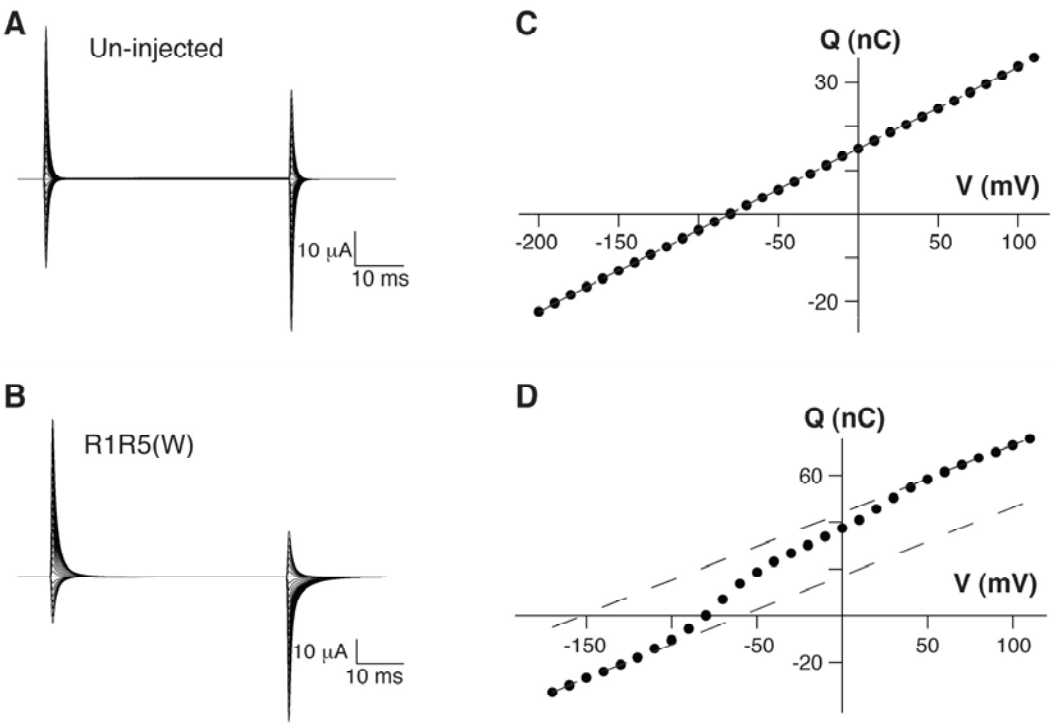

Fig. S3. Measurement of gating currents. (A-B) Transient currents measured from an uninjected oocyte (A) and an oocyte expressing the Shaker R1R5(W) mutant channel after RNA injection (B). Ionic currents were blocked using at least 50 μM Agitoxin2. **(C-D)** Q-V plots, in which integration of the repolarization-induced transient currents over time is plotted as a function of the pulse potential, are shown for an uninjected oocyte (C) and an oocyte expressing the Shaker R1R5(W) mutant channel (D). The linear component (dashed lines) of the Q-V plot reflects the charge required to bring the membrane voltage to its new value. The nonlinear gating charge component reflects the displacement of charged amino acids in the voltage sensor.

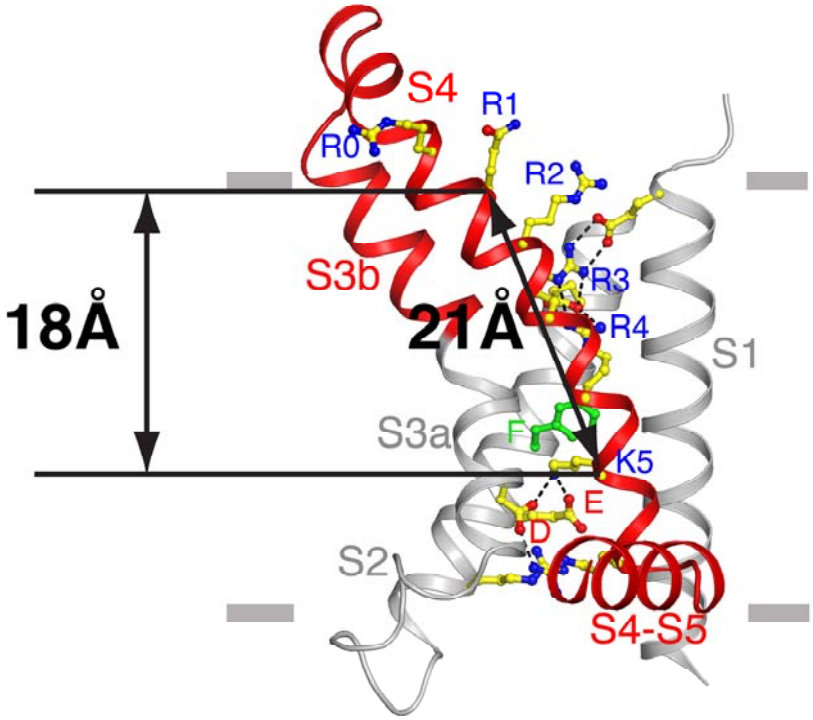

Fig. S4. Implicated voltage sensor motion. K5 binds in the occluded binding site when the voltage sensor is in its depolarized conformation in the crystal structures of Kvchim wild type and F233W mutant. The electrophysiological data suggest that Lys at position 1 binds in the occluded site in the hyperpolarized conformation. This would imply a 21 Å (α-carbon distance between R1 and K5 along the S4 helix, corresponding to 18 Å perpendicular to the membrane) distance over which the S4 charged residues move across the membrane associated with gating. The voltage sensor of Kvchim (PDB ID 2R9R) is shown as in Figure 1C.

Table S1 Crystallographic data and refinement statistics

Data collection	
Space group	P42(1)2
Lattice constants (Å)	a = b = 144.271, c = 284.060
	$\alpha = \beta = \gamma = 90°$
Source	BNL X29
Wavelength (Å)	1.0809
Resolution (Å)	50-2.9
Total / unique observations	560,259 / 67,020
I / sigma (I) [a]	17.6 (1.7)
Redundancy	8.4 (6.6)
Completeness (%)	99.5 (96.2)
R_{sym} (%) [b]	12.9 (67.5)
Model refinement	
Resolution (Å)	50-2.9
Number of reflections	66,928 (3,228)
R_{work} / R_{free}	21.1 / 24.7
R.m.s. deviation of bond length (Å)	0.007
R.m.s. deviation of bond angles (°)	1.2

R.m.s., root mean-squared.

[a]Number in the parentheses represents statistics for data in the highest resolution shell, same for redundancy, completeness, and R_{sym}.

[b]$R_{sym} = \Sigma|I_i - \langle I_i \rangle| / \Sigma I_i$, where $\langle I_i \rangle$ is the average intensity of symmetry equivalent reflections.

References

1. **S. B. Long, X. Tao, E. B. Campbell, R. Mackinnon, *Nature* 450, 376 (Nov 15, 2007).**
2. **Z. Otwinowski, W. Minor, *Methods Enzymol.* 276, 307 (1997).**
3. **N. Collaborative Computational Project, *Acta Cryst.* D50, 760 (1994).**
4. **A. T. Brunger *et al.*, *Acta Cryst.* D54, 905 (1998).**
5. **T. A. Jones, J. Y. Zou, S. W. Cowan, M. Kjeldgaard, *Acta Cryst.* A47, 110 (1991).**
6. **W. L. DeLano, *DeLano Scientific, Palo Alto, CA, USA. http://www.pymol.org*, (2002).**
7. **A. Kamb, J. Tseng-Crank, M. A. Tanouye, *Neuron* 1, 421 (Jul, 1988).**
8. **T. Hoshi, W. N. Zagotta, R. W. Aldrich, *Science* 250, 533 (Oct 26, 1990).**
9. **M. W. Nowak *et al.*, *Methods Enzymol* 293, 504 (1998).**
10. **M. E. Saks *et al.*, *J Biol Chem* 271, 23169 (Sep 20, 1996).**
11. **D. Schmidt, R. MacKinnon, *Proc Natl Acad Sci U S A* 105, 19276 (Dec 9, 2008).**
12. **S. K. Aggarwal, R. MacKinnon, *Neuron* 16, 1169 (Jun, 1996).**
13. **S. Mecozzi, A. P. West, Jr., D. A. Dougherty, *Proc Natl Acad Sci U S A* 93, 10566 (Oct 1, 1996).**